



A Coupled Thermo-mechanical Modelling Strategy Based on Alternating Direction Implicit Formulation for the Simulation of Multilayered CFRTP Thermo-stamping Process

Nicolas Bigot¹ · Edouardo Guzman-Maldonado² · M'hamed Boutaous³ · Shihe Xin³ · Nahiene Hamila⁴

Received: 28 June 2022 / Accepted: 29 August 2022 / Published online: 24 September 2022
© The Author(s), under exclusive licence to Springer Nature B.V. 2022

Abstract

A new thermo-mechanical strategy for modelling the thermo-stamping process of multilayered Carbon Fiber Reinforced Thermo-Plastics (CFRTP) materials is presented. It was derived from the use of a new two-dimensional thermo-mechanical finite element comprising a mechanical shell element covered by a thermal element based on the Alternating Direction Implicit (ADI) formulation. As a result, it was possible to solve a two-dimensional thermo-mechanical problem while obtaining the temperature distribution in the thickness direction of each layer. Applied to a viscohyperelastic constitutive law, a new invariant was proposed to model in-plane transverse elongations in unidirectional (UD) composite parts. The numerical simulation of the thermo-stamping process of a bi-layer UD PA66/Carbon Fiber prepreg revealed the potential of the presented approach. The new invariant was able to capture the anisotropic mechanical response of UD prepregs according to the orientation of the fibers. Furthermore, the ADI formulation made it possible to identify the distribution of the heat due to the contact between the prepregs and the tools through a thickness of several layers.

Keywords Composite materials · Finite element analysis (FEA) · Prepregs · Thermoforming · Thermo-mechanical · Modelling · Alternating direction implicit (ADI)

✉ Nahiene Hamila
nahiene.hamila@enib.fr

¹ LaMCoS UMR 5259, Université de Lyon, INSA-Lyon, 27 Av. Jean Capelle, F-69621, 69100 Villeurbanne, France

² Innovamics, 87 Av. des Freres Perret, 69190 Saint-Fons, France

³ CNRS, INSA-Lyon, CETHIL, UMR 5008, F-69621, Université de Lyon, 69100 Villeurbanne, France

⁴ Ecole Nationale d'Ingénieurs de Brest, ENIB, UMR CNRS 6027, IRDL, F-29200 Brest, France

1 Introduction

Fiber-based composites with thermoplastic polymer matrix meet many of today's needs. The combination of high stiffness and low density that composites offer is particularly attractive for making a structure lighter without being at the expense of performance. Large structures can be processed quickly and at a lower cost than thermoset composites, which require longer cure cycles. The thermo-stamping process is an example of a fast and industrially attractive forming process.

During the forming process, the stack of prepreg laminates is first heated to a temperature above the melting temperature of the matrix by means of a specific device, usually an infrared source. Indeed, semicrystalline polymers experience a crystallization process during which the constitutive macromolecules freeze in organized structures called crystals. As a result, the mobility of the macromolecules is limited and the material appears to be rigid. At higher temperature, the melting process occurs when enough thermal energy is provided to the material to free the macromolecules. Consequently, the material is softer. At this temperature, during the forming phase, the softening of the matrix allows shaping the composite part inside a mold preheated to a temperature lower than the crystallization temperature. This temperature is often carefully chosen to optimize the forming cycle time while ensuring the quality of the final part. Since the mold is colder than the prepreg laminate stack, thermal shock occurs at the interface. Due to the high thermal inertia characteristic of the polymer matrix, the outer layers are affected before the inner layers. This results in a strong thermal gradient, normal to the surface plane.

Most numerical simulations of composite forming are based on isothermal conditions, with temperatures of the order of the melting temperature of the thermoplastic matrix [1–7]. However, several studies [8, 9] have shown the limitations of this simplification. For example, wrinkles appear to be more numerous as the crystallization temperature approaches and the maximum shear angle increases with lower temperature. Thus, it appears that small changes in temperature can result in a significant change in the mechanical properties of the composite material.

To this extent, a solution strategy has been established to consider the underlying non-linear transient thermal problem. The mechanical problem and the thermal problem are solved separately. Solving the mechanical problem updates the geometry. Then, alternately, solving the thermal problem in turn updates the mechanical properties. This solving strategy has already been used in [10, 11] and is here implemented in an explicit finite element research software for composite shaping.

Rotation-free shell finite elements are used for mechanical simulation [12]. The thermoplastic laminate is considered to behave according to a viscohyperelastic law. This law assumes that the hyperelastic potential can be approximated by a sum of the main deformation modes: elongation in the warp and weft directions, in-plane shear and bending deformations. The thermodependent viscoelastic behavior demonstrated by the thermoplastic matrix is introduced in the in-plane shear mode with a generalized Maxwell model. These tools have already been used to simulate the forming stage of thermoforming process for complex parts composed of several prepreg layers with different orientations [9].

Based on mechanical shell finite elements, the temperature field only needs to be known in the plane direction to update the thermo-mechanical properties. Therefore, basic thermal shell elements can be used. However, modelling the heat transfer through multiple layers will require information in the thickness direction, especially to get accurate contact temperatures between each layers. A new dilemma arises. On one hand, thermal shell elements

use must be kept to elaborate a consistent and efficient thermo-mechanical strategy. On another hand, a three-dimensional thermal information is required. To this end, the Alternate Direction Implicit (ADI) formulation is applied [13]. Based on the assumptions of a strong thermal gradient and plane dimensions larger than the thickness, the ADI formulation splits the resolution of a three-dimensional thermal problem into the resolution of two-dimensional and one-dimensional problems according to in-plane and through-thickness directions respectively. As a result, the two-dimensional in-plane thermal problem shares elements and nodes of the two-dimensional mechanical problem. The shell formulation remains. The one-dimensional problem is allocated to virtual nodes and elements. A three-dimensional thermal information is reachable.

In this article, a new invariant responsible for the transverse elongation behavior is presented. A new thermo-mechanical element based on a two-dimensional mechanical element overlapped by a thermal element using the ADI formulation is described. The management of the thermo-mechanical tool/ply and ply/ply contact is explained. Finally, the numerical simulation of a two-layer UD prepreg with PA66/carbon fibers using the presented tools is carried out.

2 Modelling Strategy

2.1 Thermomechanical Modelling for Woven and Unidirectional Reinforcements

As a starting point, this paper aims at modelling the mechanical behavior of unidirectional composite layers. UD layers have the particularity to produce a soft behavior in the direction transverse to the fibers, close to the behavior of the polymer matrix. Composite parts made with multiple stack unidirectional layers by varying the directions of the fibers from one layer to another in order to obtain a tailored material. In order to generalize the viscohyperelastic constitutive laws already developed for woven composites, a new invariant must be formulated to take into account the new transverse behavior exhibited by UD layers.

The mechanical behavior is modelled using a non-linear visco-hyperelastic model [9, 14]. The membrane and bending contributions to the strain energy potential are decoupled, given the fibrous nature of one single ply. However, a specific shell approach is necessary for the modelling of multi-layered textile composites [15].

$$w = w_{\text{mem}} + w_{\text{ben}} \quad (1)$$

The membrane strain energy is expressed as a function of the physical invariants [16] associated with the different deformation modes of the reinforcement.

For orthogonal woven reinforcements, three different modes are identified: the elongation in warp direction (Fig. 1a), the elongation in weft direction (Fig. 1b) and the in-plane shear mode (Fig. 1c) [17, 18].

I_{4i} and I_{4ij} are the mixed invariants from a material having an orthogonal symmetry. C being the Cauchy-Green strain tensor and $L_{ij} = L_i \otimes L_j$ the structure tensors defined from the initial material directions L_1 and L_2 respectively the initial warp and weft direction.

The same approach can be used to model the behavior of unidirectional (UD) reinforcements. The main modes of membrane deformation for this material are assumed to be: fiber elongation (Fig. 3a), transverse elongation (Fig. 3b) and inplane shear (Fig. 3c).

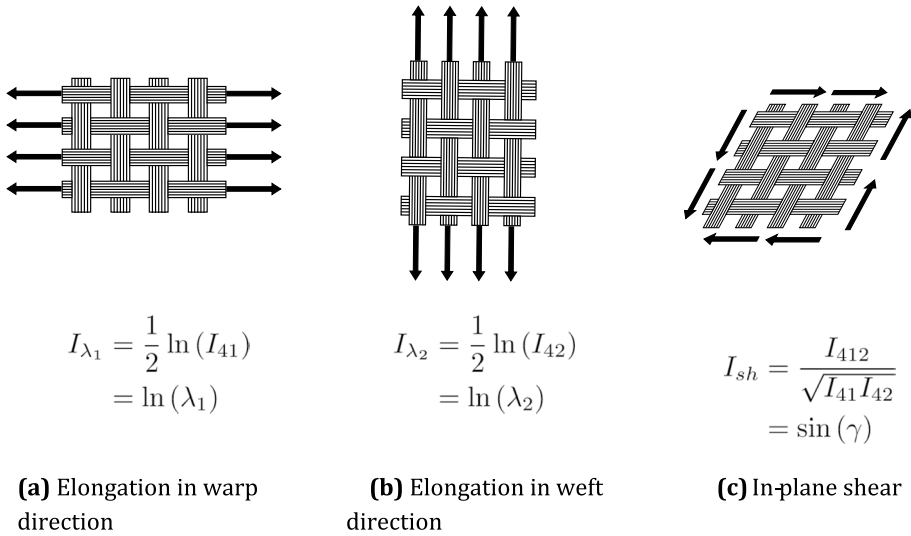


Fig. 1 In-plane deformation mechanisms in woven fabrics and their invariants

In-plane shear for UD reinforcements can be described using the same invariant as for the orthogonal case. However, the physical meaning is different. When an UD reinforcement is sheared, the fibers tend to slide between each other rather than rotate around a point, as in the case of woven fabrics [19]. In order to define a pure shear kinematic state, the shear angle γ can be defined as *the angle variation between the direction of the fibers and its perpendicular direction in the initial configuration*.

$$\gamma = \angle(\mathbf{L}_1, \mathbf{L}_2) - \angle(\mathbf{l}_1, \mathbf{l}_2) = \frac{\pi}{2} - \angle(\mathbf{l}_1, \mathbf{l}_2) \tag{2}$$

$\mathbf{l}_i = \mathbf{F}\mathbf{L}_i$ are the current material directions (Fig. 2). Under this definition, the invariant I_{sh} remains the same as before (Figs. 1c and 3c).

Transverse elongation is defined as the elongation of the material in the direction perpendicular to the fibers \mathbf{l}_t .

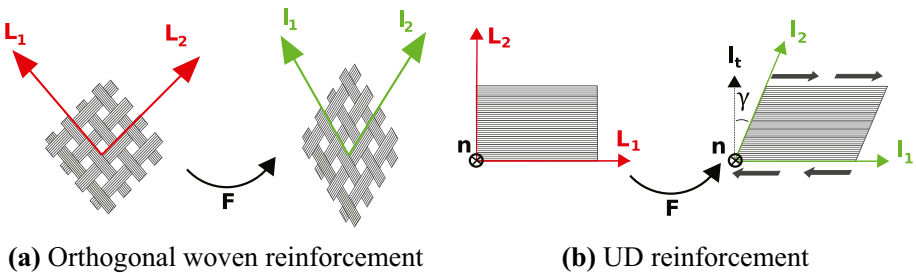


Fig. 2 Initial and deformed states of different structured reinforcements

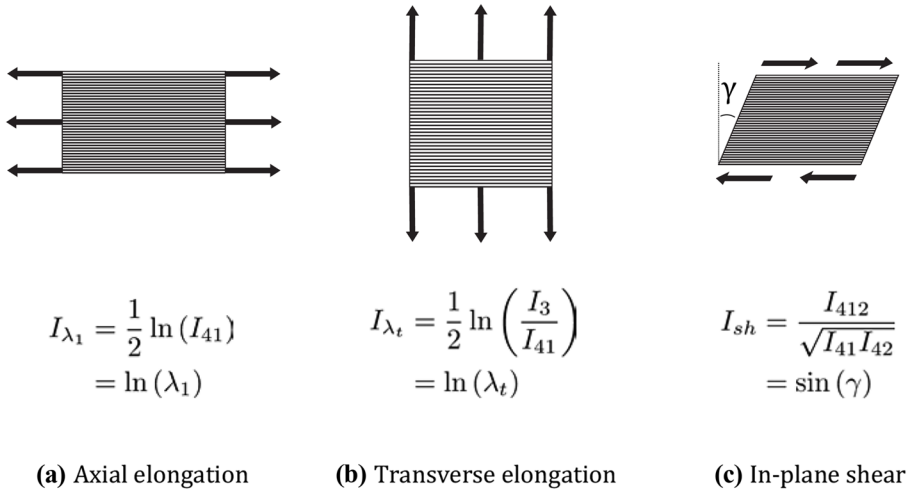


Fig. 3 Out-of-plane deformation mechanisms in composite laminates and their invariants

$$I_t = \mathbf{n} \times I_1 \tag{3}$$

\mathbf{n} being the normal unit vector to the reinforcement at each point.

An invariant, I_{λ_t} , can be defined using the definition of the classical invariant $I_3 = \det(\mathbf{C})$. Indeed, on the assumption that there is no thickness variation, the I_3 invariant is related to the variation between the initial and the current elementary surfaces, $d\mathbf{A}$ and da .

$$I_3 = \left(\frac{\|d\mathbf{a}\|}{\|d\mathbf{A}\|} \right)^2 = (\lambda_t \lambda_1)^2 = (\lambda_t)^2 I_{41} \tag{4}$$

$$I_{\lambda_t} = \ln(\lambda_t) = \frac{1}{2} \ln\left(\frac{I_3}{I_{41}}\right) \tag{5}$$

It should be noted that I_{λ_t} is independent of in-plane shear angle γ .

The fiber elongation description remains the same as that defined for orthogonal materials.

The membrane strain energy can then be expressed as a function of these physical invariants I_k .

$$w_{\text{mem}} = \sum_k w_{I_k}(I_k) \tag{6}$$

The membrane second Piola–Kirchhoff stress tensor (PK2) is obtained from the classical relation of hyperelasticity theory.

$$\mathbf{S} = \frac{1}{2} \frac{\partial w_{\text{mem}}}{\partial \mathbf{C}} \tag{7}$$

Using Eq. 1, the contributions to the second Piola–Kirchhoff stress tensor (PK2) of each deformation is given by:

$$S = \sum_k S_k = \frac{1}{2} \sum_k \frac{\partial w_{mem}}{\partial I_k} \frac{\partial I_k}{\partial C} \tag{8}$$

The derivative of invariants $I_{\lambda 1}$, $I_{\lambda 2}$ and I_{sh} respectively to C can be found on [9]. For the UD transverse elongation invariant, the derivative is given by:

$$\frac{\partial I_{\lambda_i}}{\partial C} = \frac{1}{2} \left(C^{-1} - \frac{1}{I_{4i}} L_{11} \right) \tag{9}$$

The temperature dependence of these types of materials is usually related to the matrix resin. Several studies have shown that the deformation modes which exhibit viscoelastic and temperature-dependent behavior are in-plane shear mode [8, 9, 20, 21], out-of-plane bending [7, 22–24] and transverse elongation [25].

Here it is considered that the viscoelastic behavior of the in-plane shear contribution is governed by the following expression:

$$S_{sh} = \int_{-\infty}^t G(t - s) \frac{d}{ds} \left[2 \frac{\partial w_{I_{sh}}}{\partial C} \right] ds \tag{10}$$

where G is a relaxation function given by:

$$G(t) = \gamma_{\infty} + \sum_{i=1}^N \exp\left(\frac{-t}{\tau_i}\right) \gamma_i \tag{11}$$

$\gamma_i \in [0, 1]$ and $\tau_i \geq 0$ represent the different viscoelastic thermodependent material parameters and the associated relaxation times.

The bending behavior of the material is described by directly relating the section bending moments M to the generalized curvature tensor in the principal warp χ_1 and weft χ_2 directions.

$$M = R\chi \tag{12}$$

R is the bending stiffness tensor. Bending stiffness in warp and weft direction can be expressed as a linear function of temperature for prepreg materials [22].

$$R_{\chi_1} = \beta_1^T T + \beta_1^B, \quad R_{\chi_2} = \beta_2^T T + \beta_2^B \tag{13}$$

2.2 Thermal Modelling

2.2.1 Transient Heat Transfer Problem

It is well known that temperature evolution is of great importance in the formation of complex structures. The temperature field is highly heterogeneous, mainly due to the evolution of the contact surfaces between the sheet metal and the forming tools. In-plane diffusion and three-dimensional effects cannot be neglected, especially when the boundary conditions evolve abruptly (in the vicinity of the cavity edge).

Thermal Equilibrium Equation Assuming that the main heat transfer mechanism is conduction, governed by an anisotropic Fourier model. The heat transfer problem is given by:

$$\rho c \frac{\partial T}{\partial t} = \nabla \cdot (\mathbf{K} \nabla T) \tag{14}$$

where \mathbf{K} is the local anisotropic conductivity tensor expressed in the basis (e_p, e_q, e_z) for a single ply, ρ its density and c_p its specific heat capacity. For thin shells, the conductivity tensor can be split into 2D in-plane conductivity tensor \mathbf{K}_s and 1D through thickness conductivity k_z .

$$\mathbf{K} = \begin{bmatrix} k_{pp} & k_{pq} & 0 \\ k_{qp} & k_{qq} & 0 \\ 0 & 0 & k_{zz} \end{bmatrix}_{(e_p, e_q, e_z)} = \begin{bmatrix} \mathbf{K}_s & 0 \\ 0 & k_{zz} \end{bmatrix}_{(e_p, e_q, e_z)} \tag{15}$$

By separating the in-plane contribution from the thickness contribution Eq. 14 can be expressed as:

$$\rho c \frac{\partial T}{\partial t} = \nabla_s \cdot (\mathbf{K}_s \nabla_s T) + \frac{\partial}{\partial z} \left(k_z \frac{\partial T}{\partial z} \right) \tag{16}$$

Boundary Conditions The laminate is closed by the lateral, superior and inferior boundaries, respectively Γ_{lat} , Γ_{sup} and Γ_{inf} . The upper and lower surfaces are subject to convection. The lateral surfaces are adiabatic:

$$\begin{aligned} \mathbf{q} \cdot \mathbf{n}_{sup} &= h_{sup} (T - T_{sup}) & \text{in } \Gamma_{sup} \\ \mathbf{q} \cdot \mathbf{n}_{sup} &= h_{sup} (T - T_{sup}) & \text{in } \Gamma_{inf} \\ \mathbf{q} \cdot \mathbf{n}_{lat} &= 0 & \text{in } \Gamma_{lat} \end{aligned} \tag{17}$$

with T_{inf} and T_{sup} the temperature imposed respectively on the lower and upper boundaries associated to their heat exchange coefficients h_{inf} and h_{sup} . In general case, the initial temperature field is not uniform and depends on the set of coordinates (p, q, z) in the basis (e_p, e_q, e_z) . It is given as:

$$T(p, q, z, t = 0) = T^0(p, q, z) \tag{18}$$

2.2.2 Alternate Direction Implicit Formulation

When two layers are in contact, the thermal boundary conditions enforced in each layer depend on the temperature of contact, i.e. the temperature at the surface of the concerned layers. A two-dimensional heat transfer problem could not give enough information on the temperature evolution in the thickness direction to accurately model the thermal contact. Indeed, the surface of a layer (the upper one for example) in contact with a tool experiences a thermal shock. The surface temperature decreases quickly. However, due to the thermal inertia of the polymer material, the other surface (the lower one) does not immediately undergo a change in temperature. If the latter surface is in contact with another layer, no thermal gradient should be observed because the two surfaces in contact should still be at the same temperature. It would not be the case with a two-dimensional resolution. In order to get an accurate temperature evolution in the thickness direction keeping a two-dimensional modelling of the mechanical problem, The Alternate Direction Implicit (ADI) is used.

The ADI formulation consists of separating the in-plane and the through-the-thickness thermal problem based on the assumption that the specific form of the conductivity matrix

\mathbf{K} can be expressed as (Eq. 15) and that the thickness dimension is smaller than the two other dimensions:

$$\left(\frac{h}{L}\right)^2 \ll 1 \tag{19}$$

The model reduction method of the three-dimensional heat transfer problem presented above (Eq. 23) comprises three steps: the additive decomposition, the operator splitting and the field recomposition. This paper does not aim at demonstrating the method since it has already been made in the article [26]. However, the main equations necessary for the comprehension of the present paper are underlined.

Additive Decomposition The first step consists in dividing the temperature field T into an in-plane and a through thickness contribution as follow:

$$T(x, y, z, t) = \langle T \rangle_z(x, y, t) + \tilde{T}_{x,y}(z, t) \tag{20}$$

$$\langle T \rangle_z = \frac{1}{h} \int_{-h/2}^{h/2} T(x, y, z, t) dz \tag{21}$$

With h the local thickness. At fixed position (x,y) , the temperature of a point at the position z in the thickness $T(x, y, z, t)$ is now characterized by the thickness mean temperature at this position in the plane $\langle T \rangle_z(x, y, t)$ and the deviation to this temperature $\tilde{T}_{x,y}(z, t)$.

Associated to the classic assumption for thin plate $h \ll L$, this decomposition highlights the fact that one component of the temperature varies quicker than the other (Eq. 22).

$$A = \frac{\|k_s\|}{\|k_z\|} \left(\frac{h}{L}\right) \ll 1 \Rightarrow \nabla_s \cdot (\mathbf{K}_s \nabla_s \langle T \rangle_z) \ll \frac{\partial}{\partial z} \left(k_z \frac{\partial \tilde{T}}{\partial z} \right) \tag{22}$$

Thereby, the two problems can be solved separately. Equation 14 can be reduced to:

$$\rho c \frac{\partial T}{\partial t} = \nabla_s \cdot (\mathbf{K}_s \nabla_s \langle T \rangle_z) + \frac{\partial}{\partial z} \left(k_z \frac{\partial T}{\partial z} \right) \tag{23}$$

Operator Splitting Based on the above assumptions, the thickness and plane problems can be solved separately. To this end, at time step t^n , the two problems must be solved successively, starting with the one-dimensional problem (Syst. 24). However, physically speaking, the two problems are still assumed to be solved simultaneously. This is why in this resolution strategy, both problems have the same time step Δt^n . The first problem (Syst. 24) is considered to be solved at t^n and finishes when the second one (Syst. 25) starts at $t^{n+1/2}$. The latter ends at t^{n+1} .

$$\begin{aligned} \rho c \frac{\partial T}{\partial t} &= \frac{\partial}{\partial z} \left(k_z \frac{\partial T}{\partial z} \right) && \text{in } \Omega \\ \mathbf{q} \cdot \mathbf{n}_{sup} &= h_{sup} (T - T_{sup}) && \text{in } \Gamma_{sup} \\ \mathbf{q} \cdot \mathbf{n}_{sup} &= h_{sup} (T - T_{sup}) && \text{in } \Gamma_{inf} \\ T &= T^n && \text{at } t = t^n \end{aligned} \tag{24}$$

At $t_{n+1/2}$, at each point of Ω , the average temperature $\langle T \rangle_z(x, y, t)$ is calculated from the previous obtained temperature field and becomes the initial condition for the in-plane problem (Syst. 25).

$$\begin{aligned} \rho c \frac{\partial T}{\partial t} &= \nabla_s \cdot (\mathbf{K}_s \nabla_s T) \quad \text{in } \Omega \\ \mathbf{q} \cdot \mathbf{n}_{lat} &= 0 \quad \text{in } \Gamma_{lat} \\ T &= T^{n+1/2} \end{aligned} \tag{25}$$

By applying the average operator to the Syst. 25, the in-plane problem to be solved (Syst. 26) is obtained with $\langle T \rangle_z(x, y, t)$ as the only variable.

$$\begin{aligned} \rho c \frac{\partial \langle T \rangle_z}{\partial t} &= \nabla_s \cdot (\mathbf{K}_s \nabla_s \langle T \rangle_z) \quad \text{in } \Omega \\ \nabla_s \langle T \rangle_z \cdot \mathbf{n}_{lat} &= 0 \quad \text{in } \Gamma_{lat} \\ \langle T \rangle_z &= \langle T^{n+1/2} \rangle_z \end{aligned} \tag{26}$$

Field Recomposition At each point of Ω , the one-dimensional problem enables to calculate the deviation $\tilde{T}_{x,y}(z, t)$ from the mean temperature $\langle T \rangle_z(x, y, t)$. The resolution strategy considers that this deviation, seen as a fluctuation term, is not impacted by the in-plane problem. In Syst. 26, the thermal problem can therefore be seen as an homogenization problem which only updates the mean temperature. During the time step dt , both values are updated separately and can now be gathered (Eq. 27).

$$\tilde{T}_{x,y}(z, t^{n+1/2}) = T(x, y, z, t^{n+1}) - \langle T \rangle_z(x, y, t^{n+1}) \tag{27}$$

3 Numerical Implementation

3.1 Explicit Mechanical Analysis

An explicit procedure is considered to solve the classical structural dynamic problem:

$$\mathbf{M}\mathbf{a}^n + \mathbf{C}^d \mathbf{v}^n + \mathbf{f}_{int}^n = \mathbf{f}_{ext}^n \tag{28}$$

where the total time of the simulation is subdivided in time steps Δt^n from $n=1$ to $n=n_e$ where n_e is the number of time steps and t_e the end time of the simulation. The time after the n-th integration is t^n .

$$t^n = t^0 + \sum_{i=1}^n \Delta t^i \tag{29}$$

Using an explicit analysis, the different variable vectors: displacement, velocities, accelerations are supposed to be known at time t^n . Their current state is given, for example, by applying the central difference method integration scheme [27]

$$\begin{aligned} \mathbf{a}^n &= \mathbf{M}^{-1} (\mathbf{f}_{ext}^n - \mathbf{f}_{int}^n - \mathbf{C}^d \mathbf{v}^{n-1/2}) \\ \mathbf{v}^{n+1/2} &= \mathbf{v}^{n-1/2} + \Delta t^{n+1/2} \mathbf{a}^n \\ \mathbf{u}^{n+1} &= \mathbf{u}^n + \Delta t^{n+1} \mathbf{v}^{n+1/2} \end{aligned} \tag{30}$$

where $\Delta t^{n+1/2} = \frac{\Delta t^{n+1} + \Delta t^n}{2}$. The external force vector \mathbf{f}_{ext} contains the different concentrated and distributed loads and the contact forces. The classical penalty method is considered to ensure contact constraints.

3.2 Explicit Thermal Analysis

The explicit scheme can be used to solve the *3D heat transfer problem* presented in previous section. As for the mechanical problem, the temperature field $T^n(x, y, z)$ is supposed to be known at time t_n . The update solution $T^{n+1}(x, y, z)$ at time t^{n+1} is given by:

$$T^{n+1}(x, y, z) = \langle T \rangle_z^{n+1}(x, y) - \tilde{T}_{x,y}^{n+1/2}(z, t^{n+1/2}) \quad (31)$$

with:

$$\tilde{T}_{x,y}(z, t^{n+1/2}) = T^{n+1/2}(x, y, z) - \langle T \rangle_z^{n+1/2}(x, y) \quad (32)$$

The resolution of the thermal problem is as follow:

1. Using the splitting strategy, a series of independent one-dimensional problems (Syst. 24) are solved at each node of the two-dimensional mesh to compute the trough thickness temperature field $T^{n+1/2}(x, y, z)$.
2. The average temperature $\langle T \rangle_z^{n+1/2}(x, y)$ is calculated for each node of the two-dimensional mesh.
3. The resulting two-dimensional temperature field acts as the current state to solve the in-plane thermal problem (Syst. 26).
4. Finally the deviation $\tilde{T}_{x,y}(z, t^{n+1/2})$ can be computed and the updated 3D thermal field $T^{n+1}(x, y, z)$ can be recomposed.

3.3 Explicit Thermo-Mechanical Analysis

The thermo-mechanical problem is solved at each time step according to the following procedure. At the beginning of a time step, the mechanical properties are deduced from the temperature field of the previous time step and the internal forces computed. Consequently, the mesh is updated, which settled the initial condition of the thermal problem at this time step. In turn, the thermal problem is solved, which provides the mechanical problem at the next time step for the temperature field.

The thermal boundary conditions are settled at the extremity of each onedirectional thermal problems (see Syst. 24). The external heat flux at the upper and lower surfaces for the one dimensional problem can be of two natures:

- Natural convection if the surface is not in contact.
- Conduction by contact if the surface is in contact with another body (tool, composite ply, vacuum bag, ...).

The latter is based on the mechanical boundary conditions. Contact detection allows to find the different surfaces that are in contact. Therefore, the thermal boundary conditions switch from the natural convection to the conduction by contact. The contact temperature and the thermal resistance are enforced to the concerned nodes as an application of the thermal contact properties.

To avoid a mapping operation, it is important to define the temperature and displacement degrees of freedom at the same spatial locations (nodes). This means that the

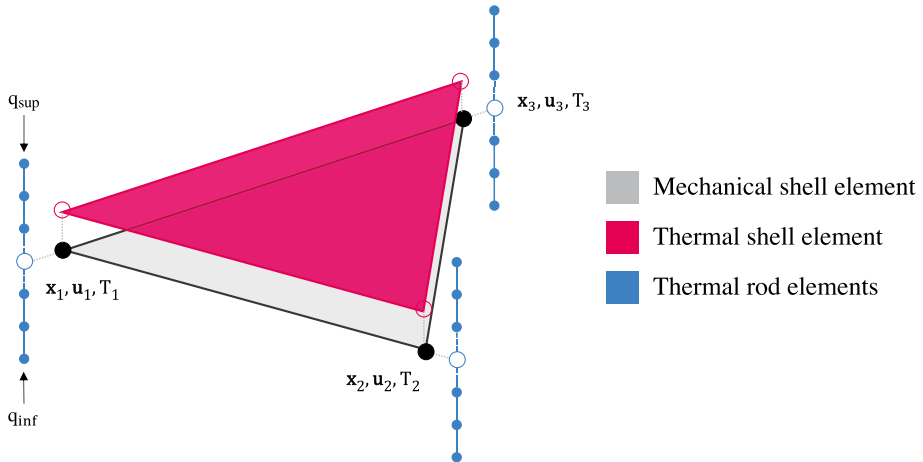


Fig. 4 Schema of the thermomechanical element composed of a mechanical membrane element overlapped with a thermal element using the ADI formulation

mechanical and thermal meshing must be compatible. A summary of the presented procedure is available in Annex as a flowchart (Fig. 12).

3.4 Virtual Thermal Elements

The simplest solution is to define the thermal mesh from the mechanical mesh. Considering a mesh with shell elements, a virtual thermal shell element is based on the mechanical element connectivity (Fig. 4). This virtual element is used to solve the two-dimensional part of the transient heat problem. Then, at each node, a one-directional transient heat problem is solved. This problem is composed by series of rod elements along a virtual line whose the length is equal to the thickness of plate. The thermal boundary conditions are only applied to the one-dimensional transient heat problems, i.e. to the nodes at both ends of the virtual line.

3.5 Contact Interfaces

3.5.1 Boundary Conditions Based on Contact Algorithm

The contact algorithm is based on the node/surface interaction using a shell approach (Fig. 5). Contact surfaces are defined using the mechanical element as the middle plane. The upper and lower contact surfaces are defined, respectively, at $+h/2$ and $-h/2$ from the middle plane. If a node penetrates the volume delimited by the contact surfaces, a contact force proportional to the distance of penetration is enforced.

The thermal contact is managed using the same approach. If a node is in contact, a heat flow is applied to the contact node. The external temperature is set to the temperature of the contact surface and a thermal contact conductance is set according to nature of the bodies in contact. This external heat flow is a boundary condition of the one-dimensional thermal ADI problem. If this node is not in contact, the heat flow is given by natural convection.

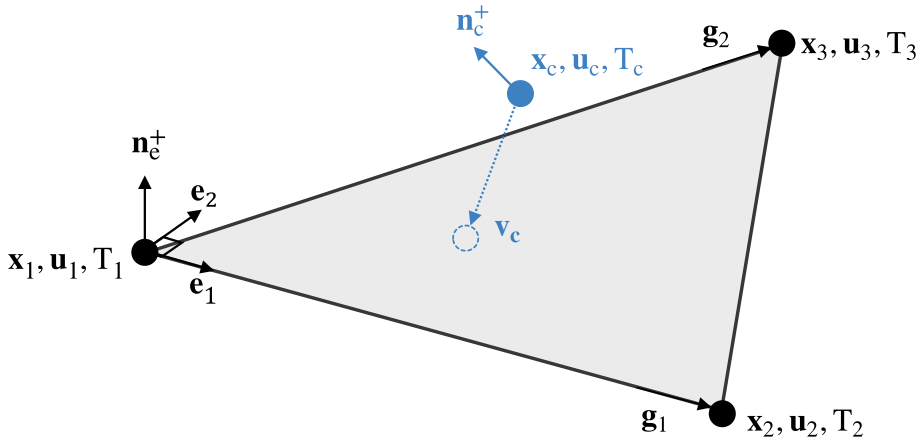


Fig. 5 Contact shell kinematics

Since the temperature through thickness is not constant, when two shell elements are in contact (e.g., layer-to-layer interaction), it is important to identify the pair of surfaces that are in contact. In Fig. 6 the different contact scenarios are shown.

By knowing the normals of each layer and their relative movement with respect to each other, a criterion can be used to identify each case of contact. For a triangular element, the positive normal can be expressed using the contravariant vectors \mathbf{g}_i .

$$\mathbf{e}_1 = \frac{\mathbf{g}_1}{\|\mathbf{g}_1\|}, \mathbf{n}_e = \frac{\mathbf{g}_1 \times \mathbf{g}_2}{\|\mathbf{g}_1 \times \mathbf{g}_2\|}, \mathbf{e}_2 = \frac{\mathbf{n}_e \times \mathbf{e}_1}{\|\mathbf{n}_e \times \mathbf{e}_1\|} \tag{33}$$

$(\mathbf{e}_1, \mathbf{e}_2, \mathbf{n}_e)$ define the local basis of the element.

However, since the contact interaction is based on a node/surface interaction, a nodal normal must be assigned to the contact node. The nodal normal can be defined by the average normal of the N_e adjacent elements sharing the same node.

$$\mathbf{n}_c^+ = \frac{1}{N} \sum_{i=1, N} \mathbf{n}_{ei} \tag{34}$$

The nodal normal \mathbf{n}_c^+ and the velocity of the contact node \mathbf{v}_c can be expressed in the local basis of the contact element:

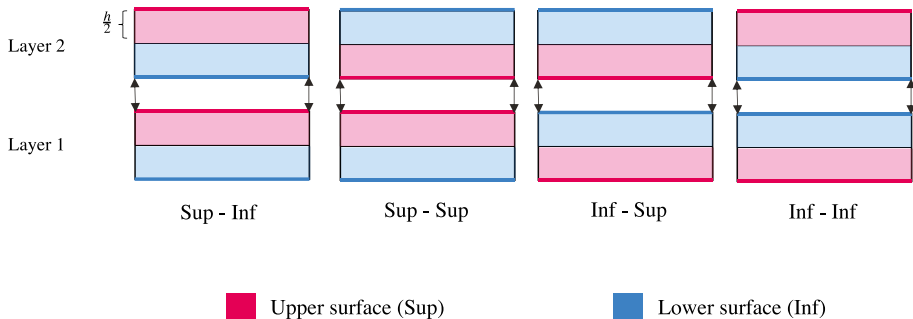


Fig. 6 Different contact interactions between two layers using a shell approach

$$\mathbf{n}_c^+ = a\mathbf{e}_1 + b\mathbf{e}_2 + c\mathbf{n}_e \tag{35}$$

$$\mathbf{v}_c = \alpha\mathbf{e}_1 + \beta\mathbf{e}_2 + \gamma\mathbf{n}_e \tag{36}$$

The projection of these two quantities onto the normal of the \mathbf{n}_e element leads to the nature of the contact between the shell elements (Table 1).

$$\mathbf{n}_e \cdot \mathbf{n}_c^+ = c \tag{37}$$

$$\mathbf{n}_e \cdot \mathbf{v}_c = \gamma \tag{38}$$

This method is independent from the nature of the finite element or the material. It is applied to the contact between two deformable surfaces or between deformable and rigid surfaces.

3.5.2 Critical Time Step

The integration scheme is conditionally stable. The critical time step in an explicit generalized central differences scheme is given by:

$$\Delta t_{\text{crit}} = \frac{2}{\omega_{\text{max}}} \tag{39}$$

With ω_{max} the maximum natural frequency of the (thermal or mechanical) system. In a conduction heat transfer problem, the equation to solve is:

$$\mathbf{K}^G \mathbf{X} = \mathbf{C}^G \mathbf{X} \boldsymbol{\omega}^G \tag{40}$$

With \mathbf{K}^G the global conductance matrix, \mathbf{X} the eigen vector matrix, \mathbf{C}^G the capacitance matrix and $\boldsymbol{\omega}^G$ the matrix of the eigen values. In order to avoid a calculation of the eigen modes, the time step can be estimated by analogy using a conduction heat problem of a rod. The critical time step is approximated by:

$$\Delta t_{\text{crit}} = \min_e \left(\frac{\rho c e^2}{6k_z \nu} \right) \tag{41}$$

With e the length of the finite element rod, k_z the thermal conductivity and ν a parameter of the integration scheme. In this case, $\nu = \frac{1}{2}$. The critical time step in general in the three-dimensional case is deduced from the smaller element of the model. The value of e for the thermal elements is given in Fig. 7.

The global critical time step of the thermomechanical problem is the smaller of the critical times between the mechanical and the thermal problem.

Table 1 Possible contact cases for shells based on the sign of c and γ

Contact case	sign c	sign γ
Sup-Inf	+	-
Inf-Sup	+	+
Sup-Sup	-	-
Inf-Inf	-	+

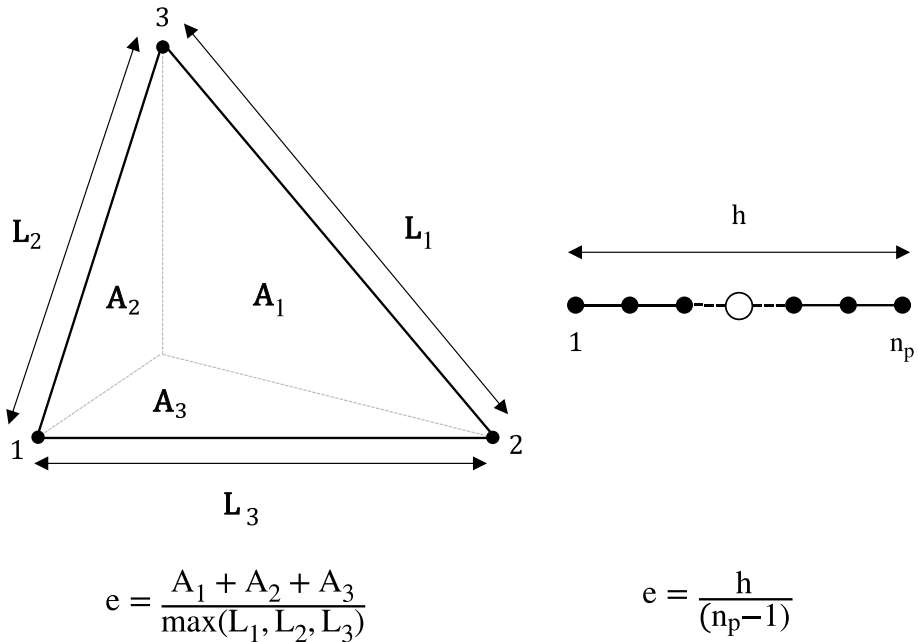


Fig. 7 Characteristic length for the thermal problems

4 Numerical Simulations

4.1 Thermo-Mechanical Simulation of the Hemispherical Test

This article proposes a numerical simulation considering the new thermomechanical element presented above. The thermal model has been validated by reproducing the results from the original article [26]. The mechanical behaviour has been validated by reproducing the results from the original article [9]. Two woven prepreg layers (160 × 160 mm) are deformed between an hemispherical punch and a perforated plate (the die). Thanks to the symmetries, only one quarter of the problem is modeled (Fig. 8).

The tool's temperature is constant and equal to 260 °C. The heating stage is not modeled in this work. The temperature of the composite part is supposed to be uniform at the beginning of the forming stage and so, of the presented simulation. The two layers of prepreg are initially at 300 °C. The cooling of the composite part is dependent on the thermal exchange with the tools, characterized by the thermal contact resistance between them set at $1 \cdot 10^{-3} \text{ m}^{-2} \text{ W}^{-1}$. No other thermal exchange is set otherwise between the tools and the prepregs in order to emphasize the effect of the thermo-mechanical contact. The prepregs have the mechanical behavior of a UD prepreg modeled with a viscohyperelastic law with thermo-dependant mechanical properties. The thermal behaviour is determined by both the PA66 and the carbon fibers thermal properties. The volume fraction of fibers is set at 40%, which is a common value encountered in the industry. The thermal properties of the carbon fibers and the PA66 are not thermo-dependant, which is relevant for the temperature between 260 °C and 300 °C. For the effective density and specific heat capacity, the rule of mixture based on a parallel model is used. The effective conductivity tensor is constructed in the local basis of a fiber such as k_{11} and k_{22} are the effective conductivity

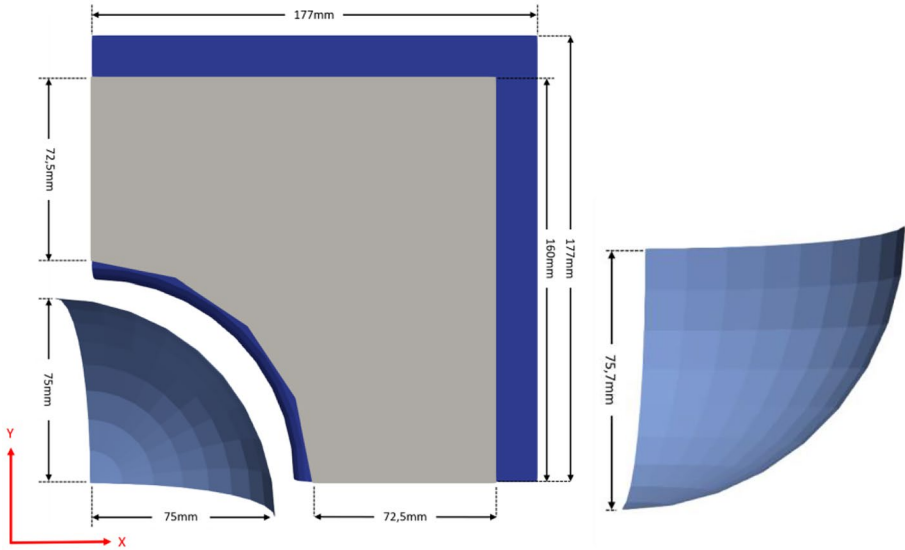


Fig. 8 Numerical simulation of the hemisphere test with the hemispherical punch (light blue), the die (dark blue), the holder (grey)

coefficient in the longitudinal and the transversely direction of the fiber respectively. k_{33} is the effective conductivity coefficient in the thickness direction. k_{22} and k_{33} are estimated based on a serial model whereas k_{11} is calculated on a parallel model. All the other coefficients are zero. Then, the effective conductivity tensor is recalculated in the global basis (e_p, e_q, e_z) according to the direction of the fibers.

Table 2 exposes the thermal parameters values with C_p the specific heat, λ the conductivity and V the specific volume equal to the inverse of the density ρ .

The mechanical parameters are found to be linearly dependent on the temperature for a range of temperature. This dependency is exhibited for parameters of Eq. 11 and for the shear potential equation, with $j=1$ if $T \leq 270$ °C and $j=2$ for $T > 270$ °C (numerical values of the parameters are gathered in Table 3) :

$$\begin{aligned}
 \gamma_j(T) &= \gamma_j^T T + \gamma_j^B \\
 \gamma_\infty &= 1 - (\gamma_1 + \gamma_2) \\
 \tau_j(T) &= \tau_j^T T + \tau_j^B \\
 \omega_{shear}(T) &= \left(\omega_j^T T + \omega_j^B \right) \sum_{i=1}^3 k_{shear}^i (I_{shear})^{2i} \\
 \omega_{warp} &= k_{warp} (I_{warp})^2 \\
 \omega_{ct} &= p_{ct} (I_{\lambda t})
 \end{aligned}
 \tag{42}$$

Table 2 Values of the thermal parameters for carbon fibers and PA66

Carbon Fibers			PA66		
Parameter	Unit	Value	Parameter	Unit	Value
ρ	kgm ⁻³	1790	ρ	kgm ⁻³	952
c	JkgK ⁻¹	800	C_p	JkgK ⁻¹	2650
λ	Wm ⁻¹ K ⁻¹	20	λ	Wm ⁻¹ K ⁻¹	0.15

Table 3 Values of the mechanical constants [9]

Parameter	Unit	Value	Parameter	Unit	Value
γ_1^T	$^{\circ}\text{C}^{-1}$	$-1.793 \cdot 10^{-3}$	ω_2^B	–	2.206
γ_1^B	–	1.397	β_1^T	$^{\circ}\text{C}^{-1}$	$-1.838 \cdot 10^{-2}$
γ_2^T	$^{\circ}\text{C}^{-1}$	$0.6845 \cdot 10^{-3}$	β_1^B	–	6.438
γ_2^B	–	$-1.491 \cdot 10^{-1}$	β_2^T	$^{\circ}\text{C}^{-1}$	$-1.838 \cdot 10^{-2}$
τ_1^T	$\text{s}^{\circ}\text{C}^{-1}$	$1.706 \cdot 10^{-1}$	β_2^B	–	6.438
τ_1^B	s	-3.715	<i>kwarp</i>	MPa	$1 \cdot 10^3$
τ_2^T	$^{\circ}\text{C}^{-1}$	$-4.527 \cdot 10^{-2}$	<i>pct</i>	MPa	$1 \cdot 10^{-1}$
τ_2^B	s	$-4.642 \cdot 10^1$	<i>kshear1</i>	MPa	$6.122 \cdot 10^{-1}$
ω_1^T	$^{\circ}\text{C}^{-1}$	$-6.010 \cdot 10^{-2}$	<i>kshear2</i>	MPa	$6.794 \cdot 10^{-1}$
ω_1^B	–	$1.663 \cdot 10^1$	<i>kshear3</i>	MPa	$-3756 \cdot 10^{-2}$
ω_2^T	$^{\circ}\text{C}^{-1}$	$-6.709 \cdot 10^{-3}$			

4.2 Mechanical Deformation

In Fig. 9b, the deformation is shown for a UD prepreg with the fiber orientation aligned with $[0, 1, 0]_{(x,y,z)}$. In this direction, the fibers are almost undeformable compared to the perpendicular direction. Indeed, in this latter direction, the deformation is absorbed by the polymer matrix which is a softer material. The fiber orientation being neither parallel nor

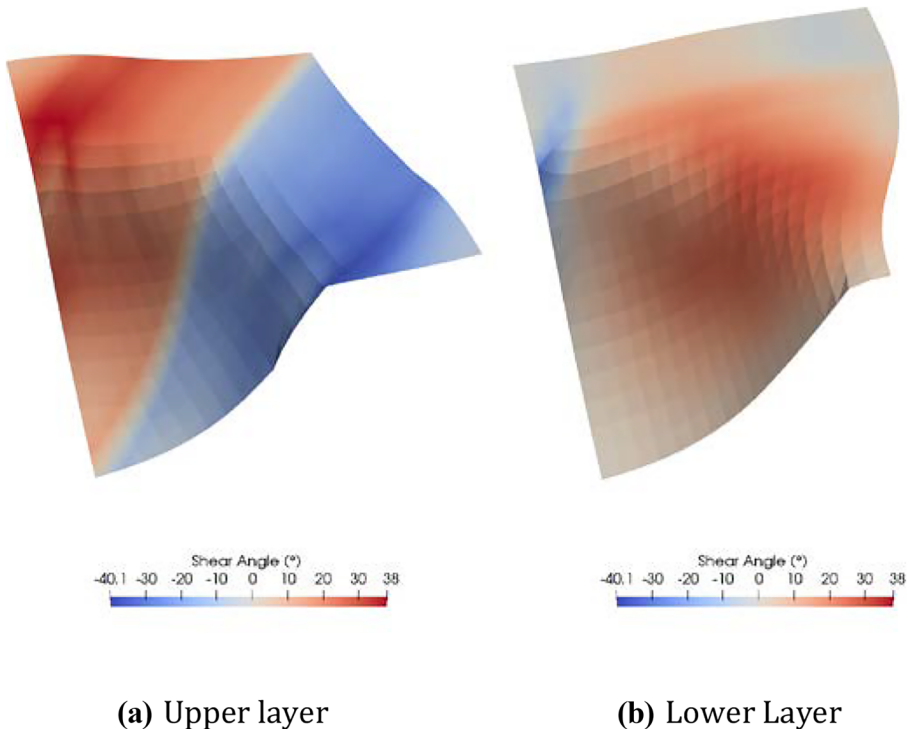


Fig. 9 Shear angle field within the two layers

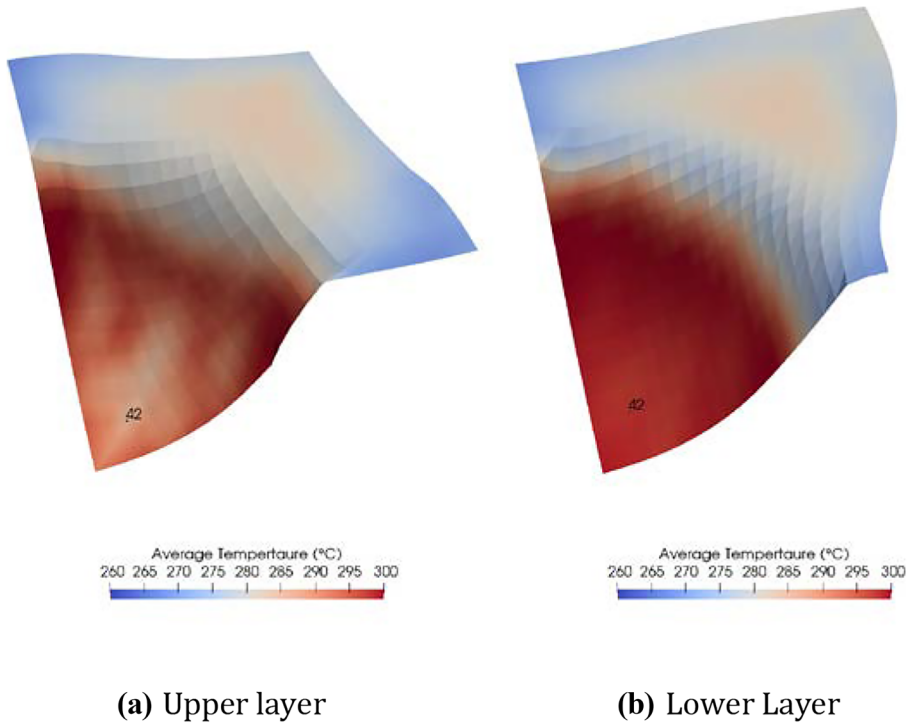


Fig. 10 Average Temperature distribution within each of the two layers

perpendicular to the symmetry axis $[1, -1, 0]_{(x,y,z)}$, an asymmetrical part is clearly obtained. This result is also confirmed by the shear angle field experienced by the part.

In relation with the results in Fig. 9b, the influence of the orientation of the fibers is emphasized in Fig. 9a. From now on, the fiber orientation is initially perpendicular to the symmetry axis of the problem and remains so during the process. It results in a symmetrical properties seen by the part and also captured by the shear angle field. The positive and

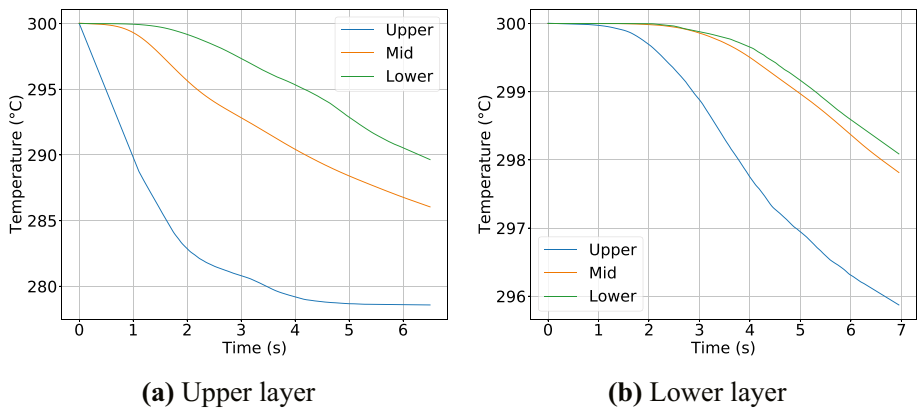


Fig. 11 Temperature distribution in the thickness direction—Node position 42

negative shear angle extrema are nearly identical in absolute value. Moreover, the positive and negative values of shear angle are separated by the symmetry axis of the problem.

4.3 Temperature Distribution

In Fig. 10a and in Fig. 10b the average temperature field is given for the upper and the lower layers respectively. Each layer is in contact with the other and with the rigid parts whose the temperature is fixed. The thermal prints of the holder and the die are clearly visible on the upper and the lower layers respectively. However, the most interesting feature is the thermal print of the punch on each layer although there is only a direct contact with the upper layer. That means there is a heat flow due to the contact with the punch which passes through the upper layer to impact the lower one. This is even more obvious on Fig. 11a and b which shows the temperature distribution in the thickness in the zone represented by the node 42 (see on Fig. 10a and b). The simulation has been able to identify the nodes in contact with a rigid part. This does not concern any nodes from the lower layer apart from those in contact with the die. That confirms that the temperature evolution on Fig. 11b is only due to the contact with the upper layer.

The previous results demonstrate the ability of the presented thermo-mechanical element to handle thermo-mechanical problems with thermo-mechanical contacts. The main feature is the ability of the thermal part of the element to represent a non-linear distribution of the temperature based on the resolution of a heat transient problem.

Another method would interpolate the nodal temperature of a three-dimensional thermal element. Several two-dimensional elements could also have been positioned along the thickness direction (one shell on the upper face, on the lower face and on the mid-plane face). Then, the temperature distribution could have been interpolated from those three shell elements. In each alternative cases, the temperature distribution in the thickness direction would have been dependent on the chosen interpolation and would have not been as accurate as the presented element for the same amount of numerical resources.

5 Conclusions

This paper proposes several powerful tools to model the thermo-stamping process of composites.

In one hand, in the framework of a hyperelastic constitutive law, a new invariant has been presented. Its role is to model the transverse elongation of unidirectional composite parts. During the numerical modelling of the forming of a two-layer unidirectional composite part made of PA66/carbon fibers, this invariant showed that it was able to restore the anisotropic behavior of UDAs as a function of the fiber orientation.

In another hand, a new strategy for thermomechanical modelling of composite forming processes is used. Resolutions of the mechanical problem and the thermal problem are performed successively. A new thermomechanical element is used. It is built around a two-dimensional mechanical element covered by a thermal element using the Alternate Direction Implicit formulation.

In the context of composite material forming, the ADI formulation considers the heat transfer problem by decoupling the resolution in the thickness direction and in the plane. This formulation allows to reduce the computational cost by continuing to consider a thermal problem in two dimensions while having temperature information in the thickness direction.

Finally, the management of the thermomechanical contact is also studied in this work. The mechanical part of the contact detects the incident node and assigns it a contact force proportional to its distance from the contact element. When the incident node is detected, the thermal part of the contact activates the temperature boundary condition in the form of a thermal contact resistance and a contact temperature equal to the temperature of the contact element. Numerical modelling of the forming of a two-layer unidirectional PA66/carbon fibers composite part proves the effectiveness of the contact management. The upper layer of the composite part is cooled by the contact with the tool. The temperature distribution in the thickness direction induced by the contact is continued in the lower layer due to the contact management between the two layers.

Appendix

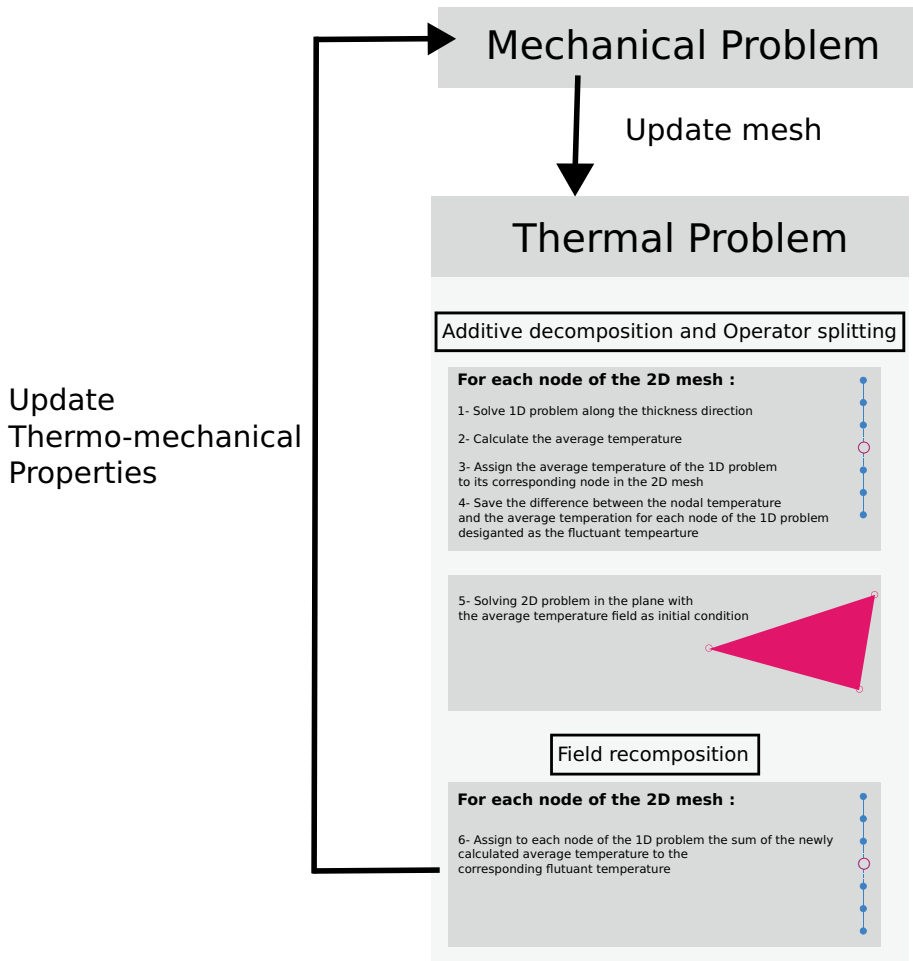


Fig. 12 Flowchart of the proposed resolution strategy for a staggered thermomechanical problem using Alternating Direction Implicit formulation

Acknowledgements The authors thank the Institut Carnot “I@Lyon” for the financial support in the framework of the project FORMICA.

Data Availability The datasets generated during and/or analyzed during the current study are available from the corresponding author on reasonable request.

References

1. Harrison, P., Gomes, R., Curado-Correia, N.: Press forming a 0/90 crossply advanced thermoplastic composite using the double-dome benchmark geometry. *Compos. A Appl. Sci. Manuf.* **54**, 56–69 (2013). <https://doi.org/10.1016/j.compositesa.2013.06.014>
2. Chen, Q., Boisse, P., Park, C.H., Saouab, A., Bréard, J.: Intra/interply shear behaviors of continuous fiber reinforced thermoplastic composites in thermoforming processes. *Compos. Struct.* **93**(7), 1692–1703 (2011). <https://doi.org/10.1016/j.compstruct.2011.01.002>. Accessed 07 Sept 2021
3. Wang, P., Hamila, N., Boisse, P.: Thermoforming simulation of multilayer composites with continuous fibres and thermoplastic matrix. *Compos. B Eng.* **52**, 127–136 (2013). <https://doi.org/10.1016/j.compositesb.2013.03.045>
4. Gong, Y., Xu, P., Peng, X., Wei, R., Yao, Y., Zhao, K.: A lamination model for forming simulation of woven fabric reinforced thermoplastic prepregs. *Compos. Struct.* **196**, 89–95 (2018). Accessed 07 Sept 2021
5. Haanappel, S.P., ten Thije, R.H.W., Sachs, U., Rietman, B., Akkerman, R.: Formability analyses of uni-directional and textile reinforced thermoplastics. *Compos. A Appl. Sci. Manuf.* **56**, 80–92 (2014). <https://doi.org/10.1016/j.compositesa.2013.09.009>
6. Machado, M., Murenu, L., Fischlschweiger, M., Major, Z.: Analysis of the thermomechanical shear behaviour of woven-reinforced thermoplasticmatrix composites during forming. *Compos. A Appl. Sci. Manuf.* **86**, 39–48 (2016). <https://doi.org/10.1016/j.compositesa.2016.03.032>. Accessed 2021-09-07
7. Dörr, D., Schirmaier, F.J., Henning, F., Kärger, L.: A viscoelastic approach for modeling bending behavior in finite element forming simulation of continuously fiber reinforced composites. *Compos. A: Appl. Sci. Manuf.* **94**, 113–123 (2017)
8. Wang, P., Hamila, N., Pineau, P., Boisse, P.: Thermo mechanical analysis of thermoplastic composite prepregs using bias-extension test. *J. Thermoplast.* **27**(5), 679–698 (2014)
9. Guzman-Maldonado, E., Hamila, N., Boisse, P., Bikard, J.: Thermomechanical analysis, modelling and simulation of the forming of preimpregnated thermoplastics composites. *Compos. A Appl. Sci. Manuf.* **78**, 211–222 (2015)
10. Tekkaya, A.E., Karbasian, H., Homberg, W., Kleiner, M.: Thermomechanical coupled simulation of hot stamping components for process design. *Prod. Eng.* **1**(1), 85–89 (2007). Accessed 07 Sept 2021
11. Brauner, C., Peters, C., Brandwein, F., Herrmann, A.S.: Analysis of process-induced deformations in thermoplastic composite materials. *J. Compos. Mater.* **48**(22), 2779–2791 (2014). <https://doi.org/10.1177/0021998313502101>. Accessed 07 Sept 2021
12. Hamila, N., Boisse, P., Sabourin, F., Brunet, M.: A semi-discrete shell finite element for textile composite reinforcement forming simulation. *Int. J. Numer. Meth. Eng.* **79**(12), 1443–1466 (2009). <https://doi.org/10.1002/nme.2625>
13. Levy, A.: Robust numerical resolution of Nakamura crystallization kinetics. *Int J Numerical Methods Eng.* (2017)
14. Guzman-Maldonado, E., Hamila, N., Naouar, N., Moulin, G., Boisse, P.: Simulation of thermoplastic prepreg thermoforming based on a viscohyperelastic model and a thermal homogenization. *Mater. Des.* **93**, 431–442 (2016)
15. Bai, R., Colmars, J., Naouar, N., Boisse, P.: A specific 3D shell approach for textile composite reinforcements under large deformation. *Compos. A: Appl. Sci. Manuf.* **139**, 106135 (2020). <https://doi.org/10.1016/j.compositesa.2020.106135>
16. Criscione, J.C., Douglas, A.S., Hunter, W.C.: Physically based strain invariant set for materials exhibiting transversely isotropic behavior. *J. Mech. Phys. Solids* **49**, 871–897 (2001)
17. Aimène, Y., E. Vidal-Sallé, B.H., Sidoroff, F., Boisse, P.: A hyperelastic approach for composite reinforcement large deformation analysis. *J. Comp. Mater.* **44**, 5–26 (2010)
18. Charmetant, a., Orliac, J.G., Vidal-Sallé, E., Boisse, P.: Hyperelastic model for large deformation analyses of 3D interlock composite preforms. *Compos. Sci. Technol.* **72**(12), 1352–1360 (2012). <https://doi.org/10.1016/j.compotech.2012.05.006>

19. Potter, K.: Bias extension measurements on cross-plyed unidirectional prepreg. *Compos. A Appl. Sci. Manuf.* **33**(1), 63–73 (2002). [https://doi.org/10.1016/S1359-835X\(01\)00057-4](https://doi.org/10.1016/S1359-835X(01)00057-4)
20. Harrison, P., Clifford, M.J., Long, A.C.: Shear characterisation of viscous woven textile composites: A comparison between picture frame and bias extension experiments. *Compos. Sci. Technol.* **64**, 1453–1465 (2004)
21. Haanappel, S., Akkerman, R.: Shear characterisation of uni-directional fibre reinforced thermoplastic melts by means of torsion. *Compos. A Appl. Sci. Manuf.* **56**, 8–26 (2014)
22. Liang, B., Hamila, N., Peillon, M., Boisse, P.: Analysis of thermoplastic prepreg bending stiffness during manufacturing and of its influence on wrinkling simulations. *Compos. A* **67**, 111–122 (2014)
23. Margossian, A., Bel, S., Hinterhoelzl, R.: Bending characterisation of a molten unidirectional carbon fibre reinforced thermoplastic composite using a Dynamic Mechanical Analysis system. *Compos. A Appl. Sci. Manuf.* **77**, 154–163 (2015)
24. Sachs, U., Akkerman, R.: Viscoelastic bending model for continuous fiberreinforced thermoplastic composites in melt. *Compos. A Appl. Sci. Manuf.* **100**, 333–341 (2017)
25. Margossian, A., Bel, S., Hinterhoelzl, R.: On the characterisation of transverse tensile properties of molten unidirectional thermoplastic composite tapes for thermoforming simulations. *Compos. A Appl. Sci. Manuf.* **88**, 48–58 (2016)
26. Levy, A., Hoang, D.A., Le Corre, S.: On the alternate direction implicit (ADI) method for solving heat transfer in composite stamping. *Mater. Sci. Appl.* **8**(01), 37 (2016)
27. Belytschko, T., Liu, W.K., Moran, B., Elkhodary, K.: *Nonlinear Finite Elements for Continua and Structures*. John Wiley & sons. (2013)

Publisher's Note Springer Nature remains neutral with regard to jurisdictional claims in published maps and institutional affiliations.

Springer Nature or its licensor holds exclusive rights to this article under a publishing agreement with the author(s) or other rightsholder(s); author self-archiving of the accepted manuscript version of this article is solely governed by the terms of such publishing agreement and applicable law.